Journal of Materials Research and Technology 30 (2024) 1159–1171

Contents lists available at ScienceDirect

Journal of Materials Research and Technology

journal homepage: www.elsevier.com/locate/jmrt

Low temperature vaporisation of Cr from fluoride flux reacted at 1350 °C with Al–Cr–Fe powder: Thermochemical analysis of gas phase reactions and nano-strand formation

Theresa Coetsee *, Frederik Johannes De Bruin

Department of Materials Science and Metallurgical Engineering, University of Pretoria, Pretoria, 0002, South Africa

ARTICLE INFO

Handling editor: P.Y. Chen

Keywords:
Welding
Slag
Fluoride
Flux
Gas
Oxy-fluoride

ABSTRACT

The submerged arc welding (SAW) process is complex because multi-phase reactions occur simultaneously across a large temperature interval from 2500 °C in the arc cavity, down to the weld pool liquidus temperare at the slag-weld pool interface. This complexity hinders research on specific process metallurgy aspects, such as gas formation from the oxy-fluoride slag. The main objective of this work is to illustrate a low temperature experimental technique as an accurate reaction simulation experiment of SAW flux oxy-fluoride slag behaviour in terms of gas formation and metal powder assimilation reaction mechanisms as observed in the SAW process. The oxy-fluoride slag behaviour was confirmed by identification and analyses of nano-strand formation in the reacted slag formed from the reaction of welding flux with Al-Fe-Cr metal powders at 1350 °C. The observed nano-strand formation agrees with similar observations in SAW post-weld slags used to confirm of oxy-fluoride vaporisation and re-condensation. Element distribution from energy dispersive X-ray spectroscopy (EDS) maps and thermochemical calculations were used to gain insights into the reactions in nano-strand formation. The nano-strands contained chromium patches and spots of less than 1 μm in scale, confirming that added Cr metal powder assimilated via the gas phase. Cr-fluoride formed part of the oxy-fluoride slag and likely formed Cr-fluoride gas. Cr was recovered via re-condensation of Cr vapour formed from the reaction of Cr-fluoride with Al gas. This work presents an accurate low temperature simulation method of gas formation and metal powder assimilation reactions in oxy-fluoride slags as in the SAW process.

1. Introduction

The process temperatures at play in the submerged arc welding (SAW) process vary over a wide range, from 2000 °C to 2500 °C in the arc cavity to the weld pool liquidus temperature at the slag-metal interface, to the solidus temperature at final weld pool solidification [1,2]. It is well established that the oxides in the SAW flux decompose in the arc cavity to release oxygen and that this oxygen can easily oxidise high oxygen affinity metals [3–5]. In recent work on the phase chemistry of SAW post-weld slags, the phenomenon of oxy-fluoride nano-strand formation within slag cavities was identified [6–8]. In this work, the conventional SAW process was modified by adding alloying metal powders and aluminium metal powder as a de-oxidiser element into the weld pool [9,10]. The metal powders were added in unconstrained format and not constrained in tubular form, as in flux cored or metal cored wires. This SAW process modification is especially useful in alloying the weld with metals of high oxygen affinity, for example, Cr and Ti metals. The main conclusion made from the work on aluminium-assisted alloying in SAW is that the gas phase reactions in the arc cavity are essential in controlling the partial oxygen pressure in the arc cavity and also the partial oxygen pressure at the slag-weld pool interface. Furthermore, it was concluded that the nano-strands observed in the slag cavities can be explained by the formation of gas species in the arc cavity. The nano-strands formed from re-condensation of the arc cavity gasses, which formed during aluminium-assisted SAW. These conclusions were reached based on phase chemistry analyses of nano-strands identified in the post-weld slags, in combination with thermochemical calculations on possible gas phase formation reactions.

Gas phase species also form in the absence of metal powder additions, that is in the conventional SAW process, as indicated in thermochemical calculations for the gas-slag-metal equilibrium at 2000 °C as CO, Na, NaF, CaF_2, MgF_2, MgF, AlF_3, AlF_2, $NaAlF_4$, TiF_3, $KAlF_4$ as major

* Corresponding author.
E-mail addresses: theresa.coetsee@up.ac.za (T. Coetsee), fjdb.1953@gmail.com (F.J. De Bruin).

https://doi.org/10.1016/j.jmrt.2024.03.100
Received 27 December 2023; Received in revised form 25 February 2024; Accepted 17 March 2024
Available online 22 March 2024

species, with minor gas species of K, KF, Mg, AlF, Mn, Fe, SiF_4, and SiO present at less than 1 vol % [11]. In aluminium-assisted SAW, the de-oxidiser function of Al is to decrease the partial oxygen pressure in the arc cavity to ensure that the alloying metals remain as metal in the weld pool and as metal vapour in the arc cavity instead of oxidising to oxides. The gas-slag-metal equilibrium calculations identified chromium metal vapour as the main chromium gas species, and only a minor amount of CrF_3 was present in the calculated gas composition made for 2000 °C and 2500 °C [7,8]. The equilibrium calculation for the modified SAW process at 2500 °C with added Al–Ni–Cr–Co–Cu metal powders identified the gas species as Mg, AlF, Fe, Cu, N_2, CO, OAlF, SiO, Mn, Na, MgF, Cr, AlF_2, Al_2O and Al [8].

The SAW process is complex because of multi-phase reactions occurring simultaneously in the arc-cavity at the high temperatures of 2000 °C–2500 °C and continued reactions occurring at the slag-metal interface at the lower temperatures of the weld pool [1,2]. These varied reaction zones and temperatures complicate research on specific process metallurgy aspects, such as gas formation from the oxy-fluoride slag. Therefore, the objective of this work is to illustrate a low temperature (1350 °C) experimental technique that is an accurate reaction simulation experiment of oxy-fluoride slag behaviour in SAW fluxes in terms of gas formation and metal powder assimilation reaction mechanisms as observed in the SAW process. Confirmation of nano-strand formation in the oxy-fluoride slag formed from low temperature reaction of welding flux with Al–Fe–Cr metal powders is required to confirm oxy-fluoride vaporisation and re-condensation as previously identified in post-weld slags generated from modified SAW with Al–Cr-metal powders additions [6–8].

2. Material and methods

An Aluminate Basic agglomerated commercial flux was applied in this work. This flux was also applied in the previous welding experiments with the analysis summarised in Table 1, and iron oxide expressed as Fe_2O_3 [6–12]. The mineralogy and chemistry of this flux and its post-weld slag were described elsewhere [12]. The slag phases consist of the liquid oxy-fluoride main phase and spinel crystals ($MgO{\cdot}Al_2O_3$) [12]. The flux agglomerate particle size was 0.2–1.6 mm.

The added pure metal powders were sourced as follows: Al (99.7% Al, −1 mm) supplied by Sigma-Aldrich, Cr (99.0% Cr, −44 μm) supplied by Alfa Aesar, Fe (96.0% Fe, −50 μm) supplied by Merck. The addition of Fe powder was made to simulate the presence of Fe in the SAW of carbon steel, as sourced from the weld wire and base plate [6–12]. The Al and Cr powders are the same as those applied in the prior SAW work [6–9].

In this work, the solid reactants of flux and metal powders were mixed and dry-pressed into a cylindrical pellet. Metal powders were added at eight mass% of the overall mixture. Before loading the pellet into the furnace, it was placed onto the pellet holder. The pellet holder consisted of a low carbon steel plate of dimensions of 65 mm square and 2 mm thickness. The pellet holder had a pressed circular recessed centre to assist in pellet placement. A muffle furnace was pre-heated to 1350 °C and then soaked for 12 h at 1350 °C. Following this soaking time, the pellet holder and pellet were placed into the muffle furnace and reacted for 6 min. Upon completion of the reaction time, the pellet was removed from the furnace to cool down in the air. The cooled pellet was sectioned through its middle, and the inner faces were coated with gold. The three-dimensional (3D) sample was analysed by scanning electron microscope (SEM). A Zeiss crossbeam 540 FEG (field emission gun) SEM with EDS (energy dispersive X-ray spectroscopy) probe operated at 20 kV was used to perform phase chemical analyses of the 3D sample.

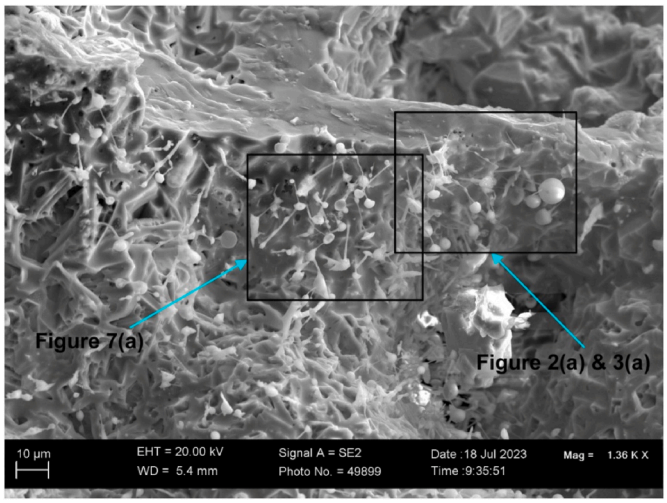

Fig. 1. BSE image of nano-strands at low magnification (x1360).

3. Results and discussion

The first priority of the SEM investigation was to confirm the formation of nano-strands in the slag. Secondly, the nano-strands' phase chemical analyses were used to gain insights into the possible formation reactions of the nano-strands by applying thermochemical analysis. The FactSage 7.3 thermochemical software was employed in the thermochemical analysis [13].

The backscattered electron (BSE) image in Fig. 1 clearly shows the presence of nano-strands. The two blocked areas in Fig. 1 were analysed at progressively higher magnifications as follows: Figs. 2–6 show features in the right-hand block of Fig. 1, and Figs. 7–10 show features in the left-hand block. The average analysis of each field of view in Figs. 2–10 is summarised in Table 2. The maximum standard deviation values (σ) shown in Table 2 indicate the SEM-EDS analysis quality. For comparison, the flux analysis from Table 1 is shown in the last line of Table 2. Similarly, the glass phase SEM-EDS analyses in post-weld slag from welding without metal powder additions are also shown in the second and third last lines of Table 2 [12]. It is clear that Al and Cr were added to the slag from the added metal powders. In contrast, the concentrations of F, Mg, Si, Mn, and Fe in the slag were lowered compared to the bulk flux analysis and the post-weld slag glass phase analyses. The analyses in Table 2 do not serve as quantification of the extent of metal loss to slag or gas because there may be metal powders remaining that have not participated in the reactions. In the prior aluminium-assisted alloying of SAW with added Cr metal powder, the Cr yields varied from 60% to 90% [7–9,14]. These Cr yield numbers may be compared to those achieved in SAW with added pre-alloyed metal powders, without Al de-oxidiser, at 56% to76% Cr yield [15]. Fig. 2(b) to 10(b) show the element maps of the field of view in the BSE images in Fig. 2(a) to 10(a). These analyses are necessary to view the distribution of each element across the morphology features shown in Figs. 2–10. The nano-strands in all of the BSE images vary with respect to strand diameter, nodes contained in the strand and the features at the end of the nano-strand positioned away from the flux surface (the gas end of the nano-strand). These ends appear as different shapes such as a sphere, petal, droplet or a pointy end. The strands appear homogenous in terms

Table 1
Chemical composition of flux material.

%MnO	%CaO	$\%SiO_2$	$\%Al_2O_3$	$\%CaF_2$	%MgO	$\%Fe_2O_3$	$\%TiO_2$	$\%Na_2O$	$\%K_2O$
7.0	0.1	20.2	25.7	18.5	22.9	2.7	1.0	1.7	0.2

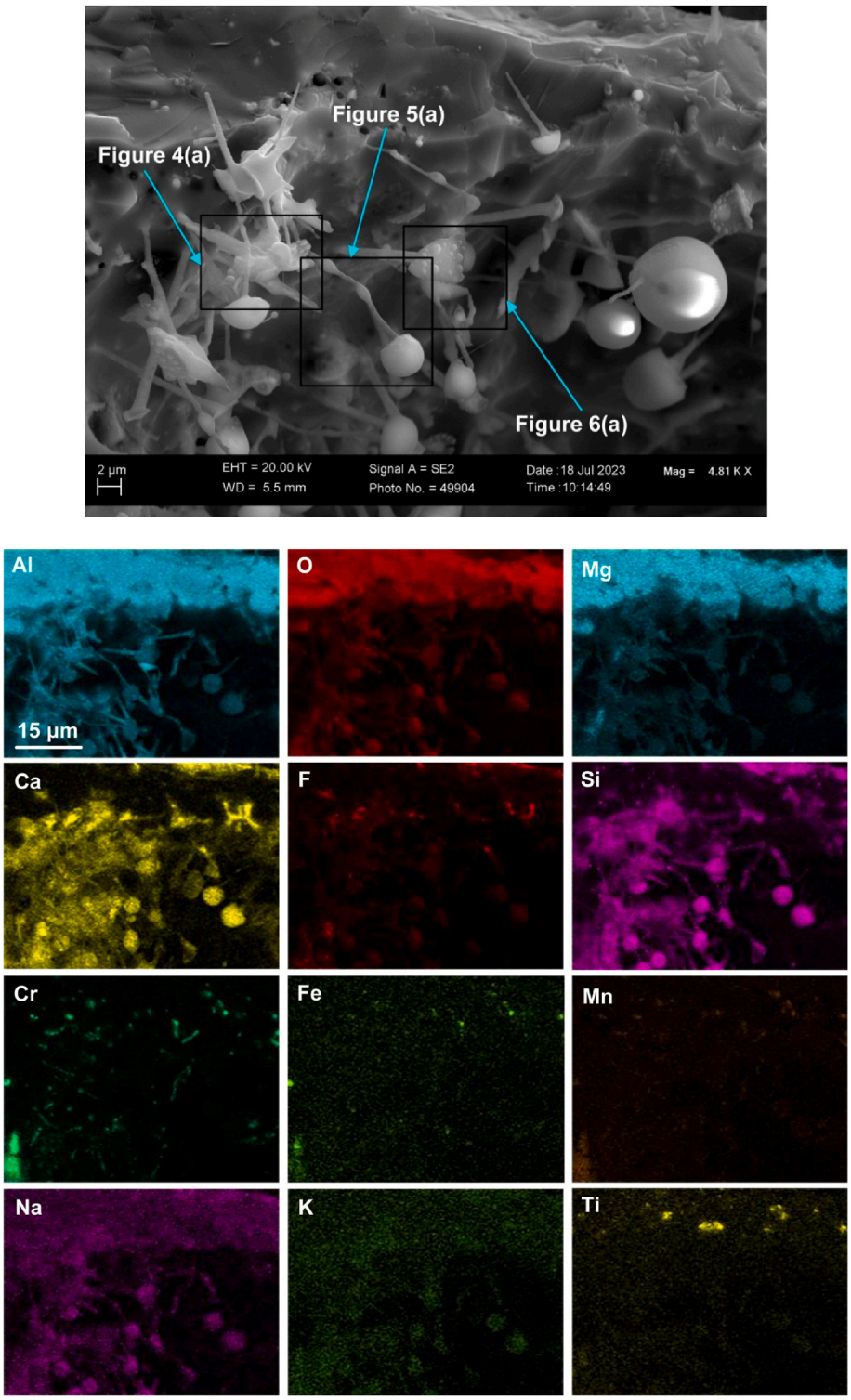

Fig. 2. (a): BSE image (x4180) of analysed area as marked in Fig. 1; (b): EDS map of area in Fig. 2(a).

of the main elements as the Al–Mg–Ca–Si–Na–K oxy-fluoride, even when nodes are present in the strand as displayed in Fig. 5. Even though little Ti is present in the flux material, Ti appears to follow the main elements into the nano-strands, as seen in Figs. 5 and 6. Chromium added as metal powder of −44 µm particle size was assimilated into the nano-strands. This effect can be seen in the nano-strands at the centre of each of Figs. 5, 6, 9 and 10. Brighter spots and patches of chromium are displayed in these figures, usually in association with Fe and Mn. These chromium patches are sometimes part of the background oxy-fluoride phase as seen in Figs. 8 and 9. However, some chromium patches and spots are also part of the nano-strand shapes as seen in Figs. 4 and 6. All of these chromium spots and patches are less than 1 µm in scale, confirming that the chromium assimilated via the gas phase. Furthermore, the nano-strand morphology seen in Figs. 1–10 appears similar to the nano-strands seen in SAW post-weld slags and is associated with oxy-fluoride vaporisation and re-condensation [6–8].

In the following section the probable gas species formation is calculated from thermochemistry using Gibbs free energy calculations.

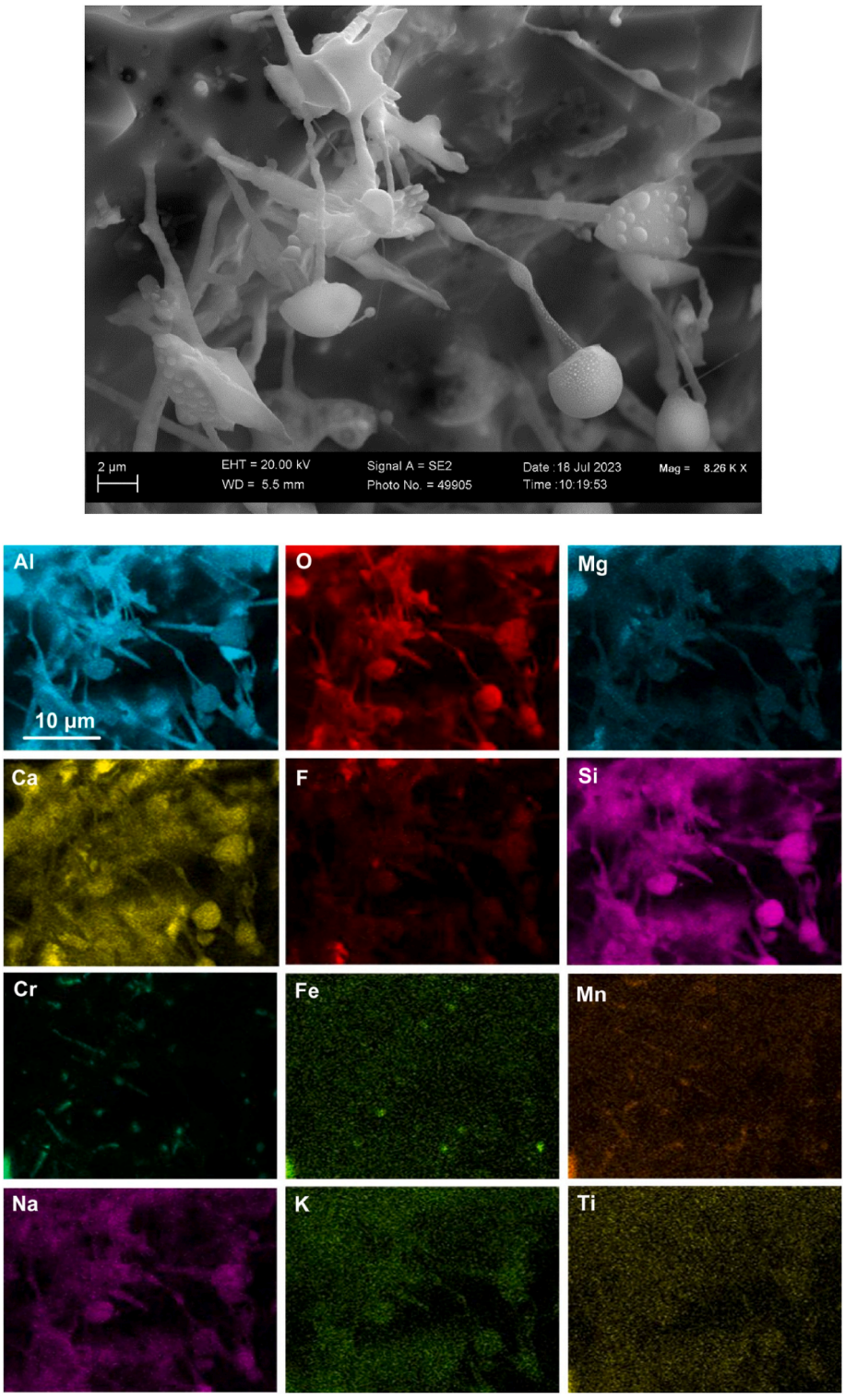

Fig. 3. (a): BSE image (x8260) of analysed area as marked in Fig. 1; (b): EDS map of area in Fig. 3(a).

The thermochemical software FactSage 7.3 was used. The Reaction module was used to calculate Gibbs free energy values of specific reactions, using the databases FactPS and FToxid. Calculations were made for 1300 °C–2000 °C to compare the relative thermodynamic favourability of the reactions at 1350 °C to that at much higher temperatures encountered in SAW. Liquid state reaction temperatures in the SAW process vary from 2000 °C to 2500 °C in the arc cavity to the weld pool liquidus temperature, in the order of 1600 °C for carbon steel [1,2].

As a first consideration, as in our previous work on SAW, we considered the vapour pressure of the pure metals, as displayed in Fig. 11 [6,7]. It is seen that K, Na and Mg have high vapour pressures, even at 1300 °C. The vapour pressures of Mn, Al, Cr, Fe and Si are lower but not insignificant. The addition of Al to the SAW reaction system was done to achieve a low partial oxygen pressure in the SAW process to maintain high oxygen affinity elements such as Cr in the metallic state [6–10]. This effect of Al addition is also at play in the current work done at lower temperature. Next, the most probable reaction of metals according to reaction (1) was investigated for this reaction system. The

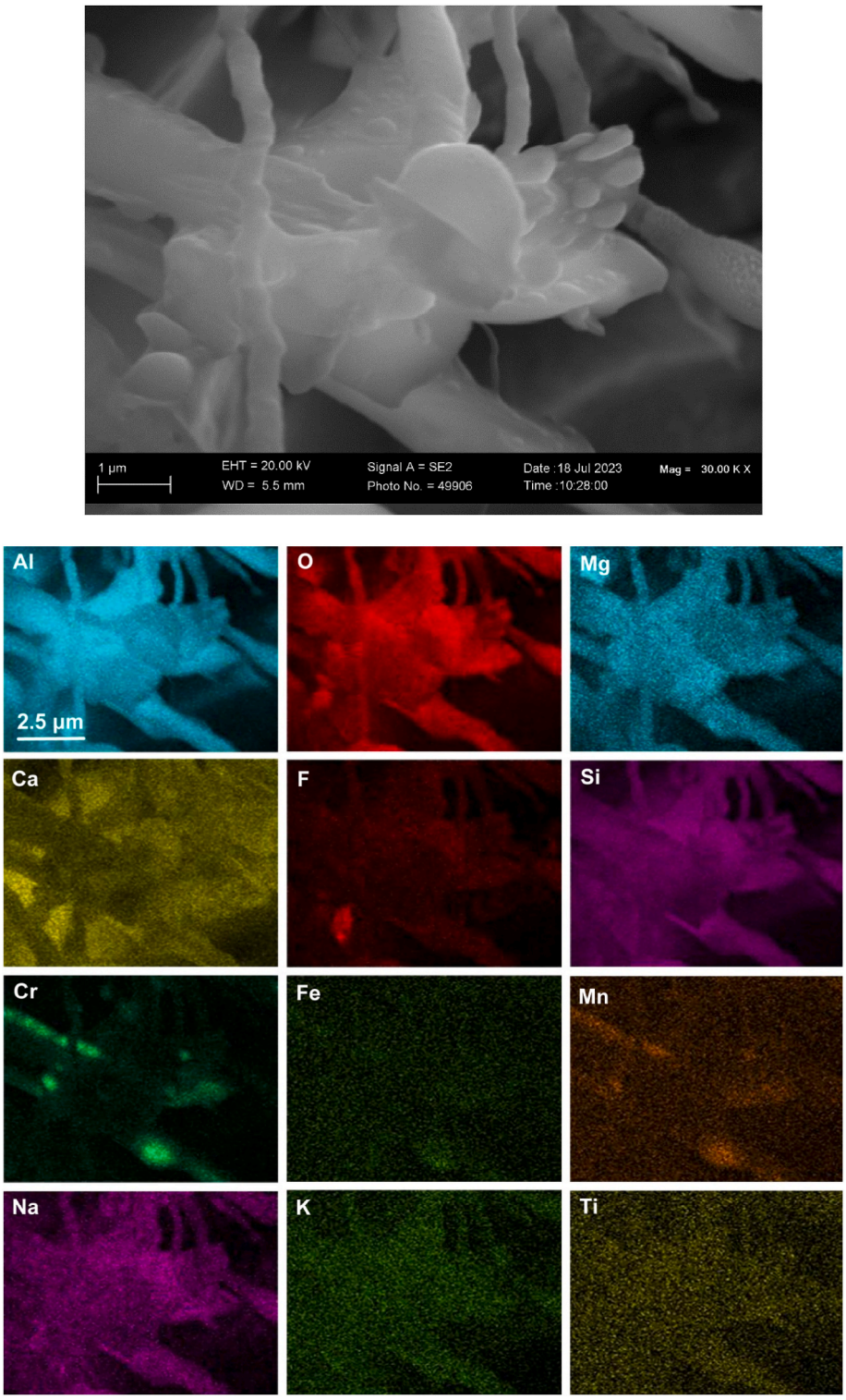

Fig. 4. (a): BSE image (x30000) of analysed area as marked in Fig. 2(a); (b): EDS map of area in Fig. 4(a).

phrase "(most stable)" refers to the selection made in the Reaction module in FactSage to change the phase state with temperature.

$$M(\text{most stable}) + (x/2)F_2(g) \leftrightarrow MF_x(\text{most stable}) \quad (1)$$

Fig. 12 shows the relative stability of fluorides formed from reaction (1). The fluorides are present as liquid or gas in the temperature range of 1300 °C–2000 °C. KF, NaF, FeF_2, and MnF_2 transition from liquid to gas as indicated by filled circle icons in Fig. 12. MgF_2 is in the liquid state in Fig. 12 since its gas transition temperature is 2263 °C. It is seen that the Gibbs free energy lines mostly hold the same order in Gibbs free energy values across the temperature range, with a few exceptions. The line for MgF_2 has a steeper slope and, therefore, crosses the lines for AlF_2 and FeF_3 at 1800 °C, indicating that MgF_2 is more stable than AlF_2 and FeF_3 below 1800 °C. The other instance of line crossing is at 1300 °C, resulting in higher stability of KF and NaF relative to AlF below 1300 °C. Overall, the stability order of fluorides is similar at 2000 °C and 1350 °C.

Because both oxides and fluorides are contained in the flux, and $F_2(g)$

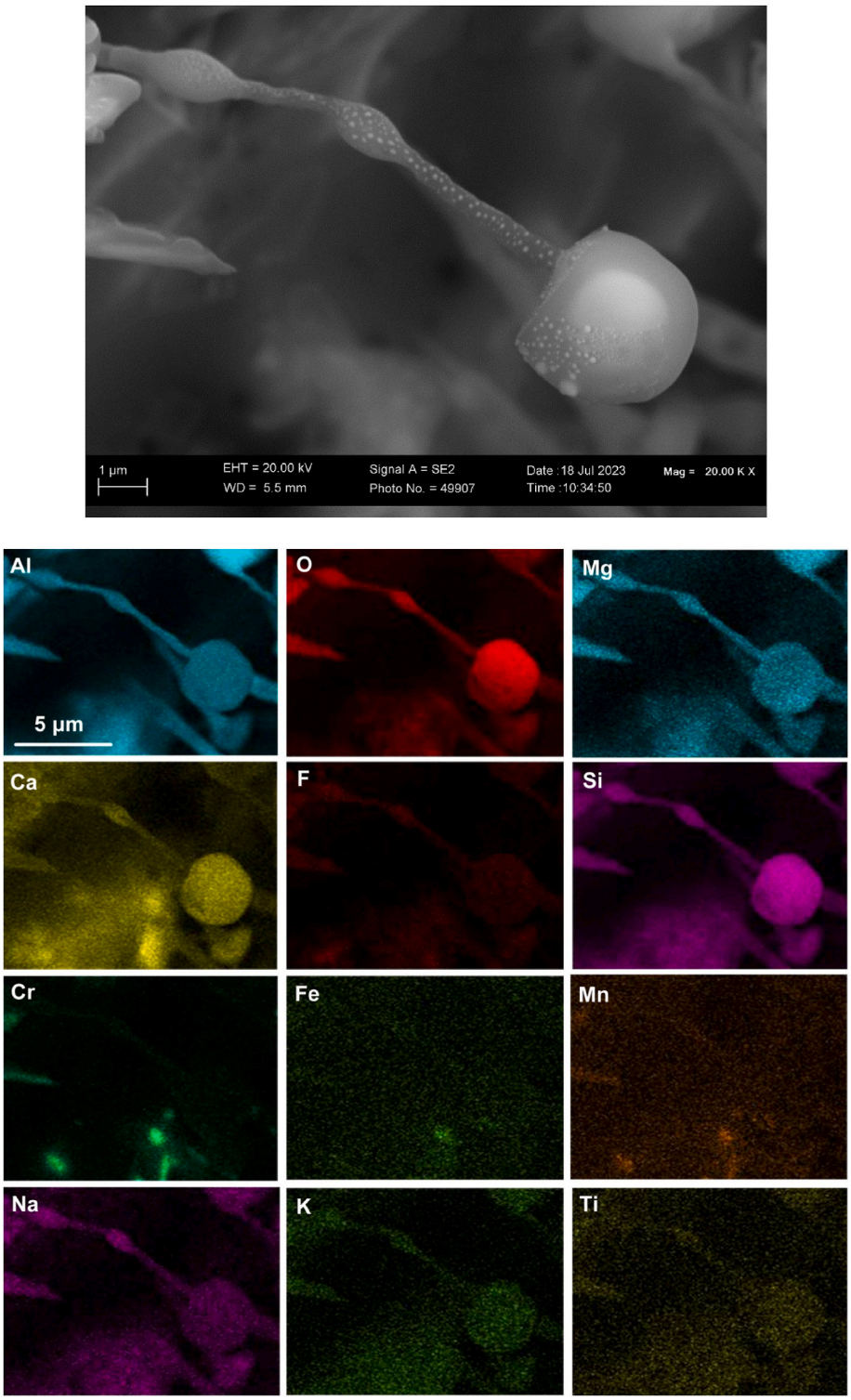

Fig. 5. (a): BSE image (x20000) of analysed area as marked in Fig. 2(a); (b): EDS map of area in Fig. 5(a).

and $O_2(g)$ are present in the arc cavity, the relative stability of oxides and fluorides is of importance in the oxy-fluoride based reaction system. A comparison of the relative affinity of metals to $F_2(g)$ and $O_2(g)$ can be seen from a comparison of the Gibbs free energy lines in Fig. 12 to those in Fig. 13. The latter figure contains the Gibbs free energy lines for the reaction of metal with oxygen, as displayed in reaction (2). Comparison of the Gibbs free energy values for the reaction of a metal with $F_2(g)$ is of a more negative value than that of the reaction of the metal with $O_2(g)$, confirming that fluoride formation is favoured ahead of oxide formation.

Aluminium has a high affinity for oxygen, as indicated by the large negative Gibbs free energy values in Fig. 13 for the reaction of Al with O via reaction (2). This is the reason for using Al as deoxidiser in the aluminium-assisted SAW process to control the oxygen partial pressure in the reaction system to lower levels than the Fe–FeO oxygen partial pressure that would otherwise dominate the reaction system [6–11]. The same approach is followed in ladle metallurgy in steelmaking to lower the dissolved oxygen in molten steel.

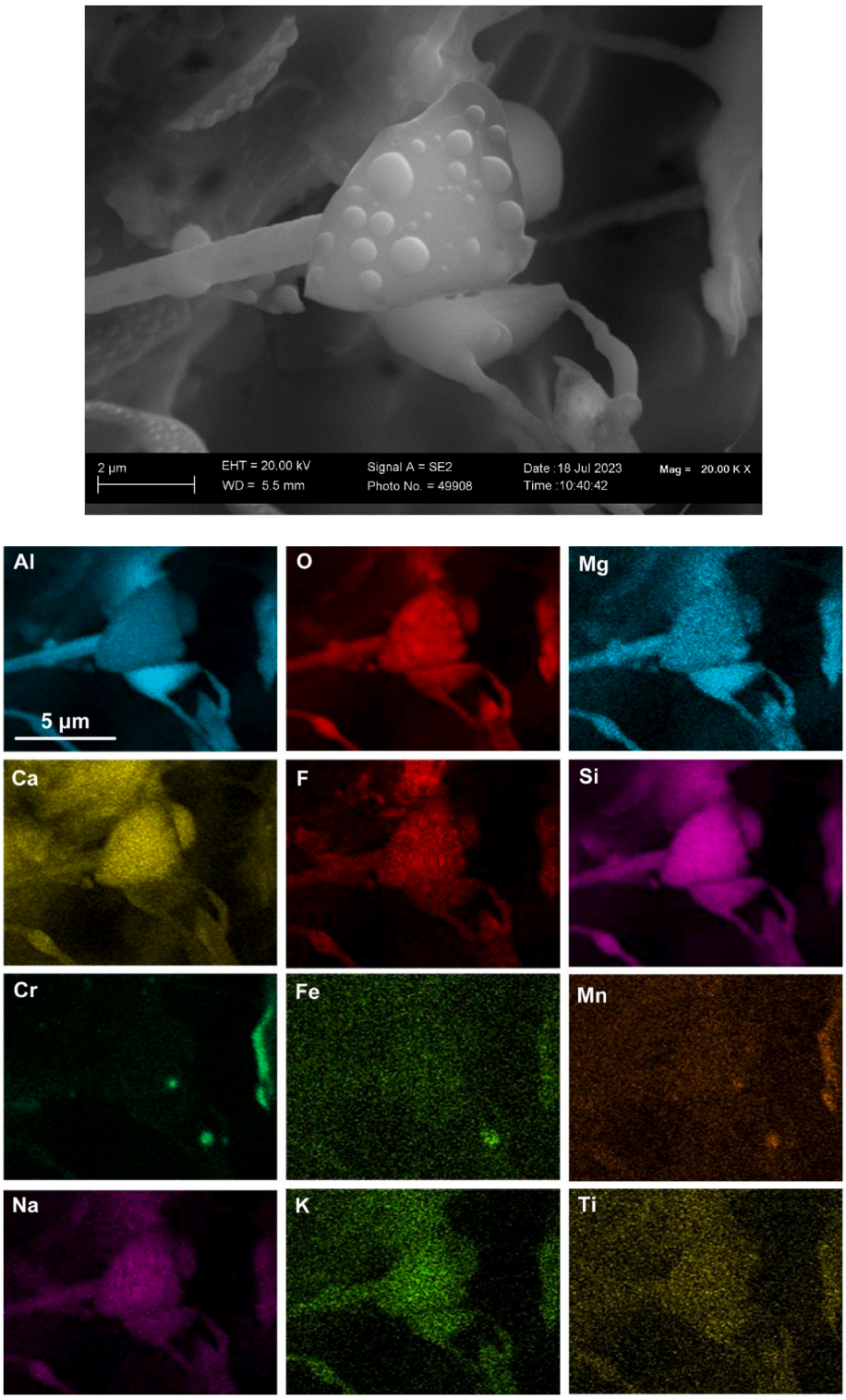

Fig. 6. (a):BSE image (x20000) of analysed area as marked in Fig. 2(a); (b): EDS map of area in Fig. 6(a).

$$M(\text{most stable}) + (x/2)O_2(g) \leftrightarrow MOx\ (\text{most stable}) \quad (2)$$

The fluoride compounds in the liquid state are not individual phases because the fluoride and oxides combine chemically into a liquid oxy-fluoride matrix phase. Similarly, the formation reactions of fluorides differ from reaction (1) because the formation of $F_2(g)$ is uncertain. Although sublimation of fluoride may be possible, it is accepted that fluorides may form from the reaction of oxides with CaF_2, as displayed in reaction (3). This reaction is generally written in SAW flux research texts for different oxides reacting with CaF_2 to form CaO and metal fluorides [3,16].

$$SiO_2(slag) + 2CaF_2(g) \leftrightarrow 2CaO(slag) + SiF_4(g) \quad (3)$$

Fig. 14 shows the Gibbs free energy for reactions similar to reaction (3) to form each metal fluoride gas product (MF_X) with inputs of 1 atm CaF_2 partial pressure; the product fluoride gas at 0.10 atm partial pressure; the activity of the liquid flux oxide in the oxy-fluoride slag was set to 0.5 and the activity of CaO set to 0.01 ($a_{CaO} = 0.01$). The activity

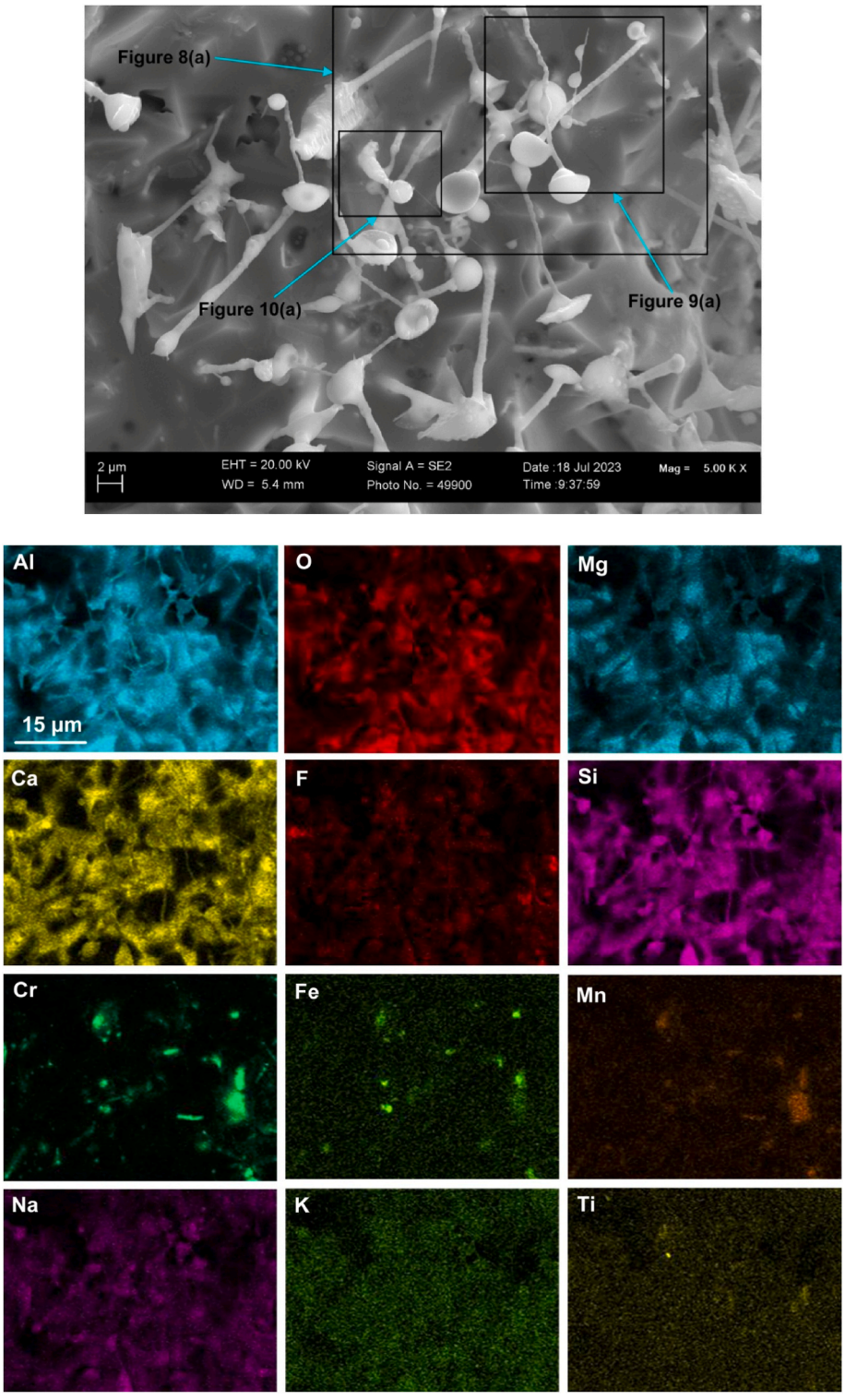

Fig. 7. (a): BSE image (x5000) of analysed area as marked in Fig. 1; (b): EDS map of area in Fig. 7(a).

and partial pressure values are based on value selections made for SAW [12]. It is seen that KF is most easily formed. The lines for the reaction of Na_2O with CaF_2 to NaF cross the line for SiF_4 formation at 1342 °C. Therefore, at 1350 °C, the formation of NaF is favoured ahead of SiF_4 formation via reaction (3). The next most probable reaction with CaF_2 at 1350 °C is the formation of FeF_3, AlF_3, CrF_3, MgF_2, MnF_2 and FeF_2.

At the high temperatures in the arc cavity, the fluorides are easily vaporised, whilst vaporisation at the lower temperatures occurs only for some of the fluorides, as shown in Fig. 12. However, the information in Fig. 12 was calculated for pure reactants, and this is not the case in a chemically complex reaction system as studied in this work since an oxy-fluoride slag is formed upon melting, and this slag contains all the fluorides and most of the oxides. The vaporisation of fluoride compounds from oxy-fluoride melts below 1400 °C is well reported in the literature, even though the gas species and reactions are not precisely known [17,18]. The formation of some oxygen-containing fluoride gas was also identified in the form of AlOF [19]. Free oxygen from air may also incorporate into the nano-strands during the re-condensation of the

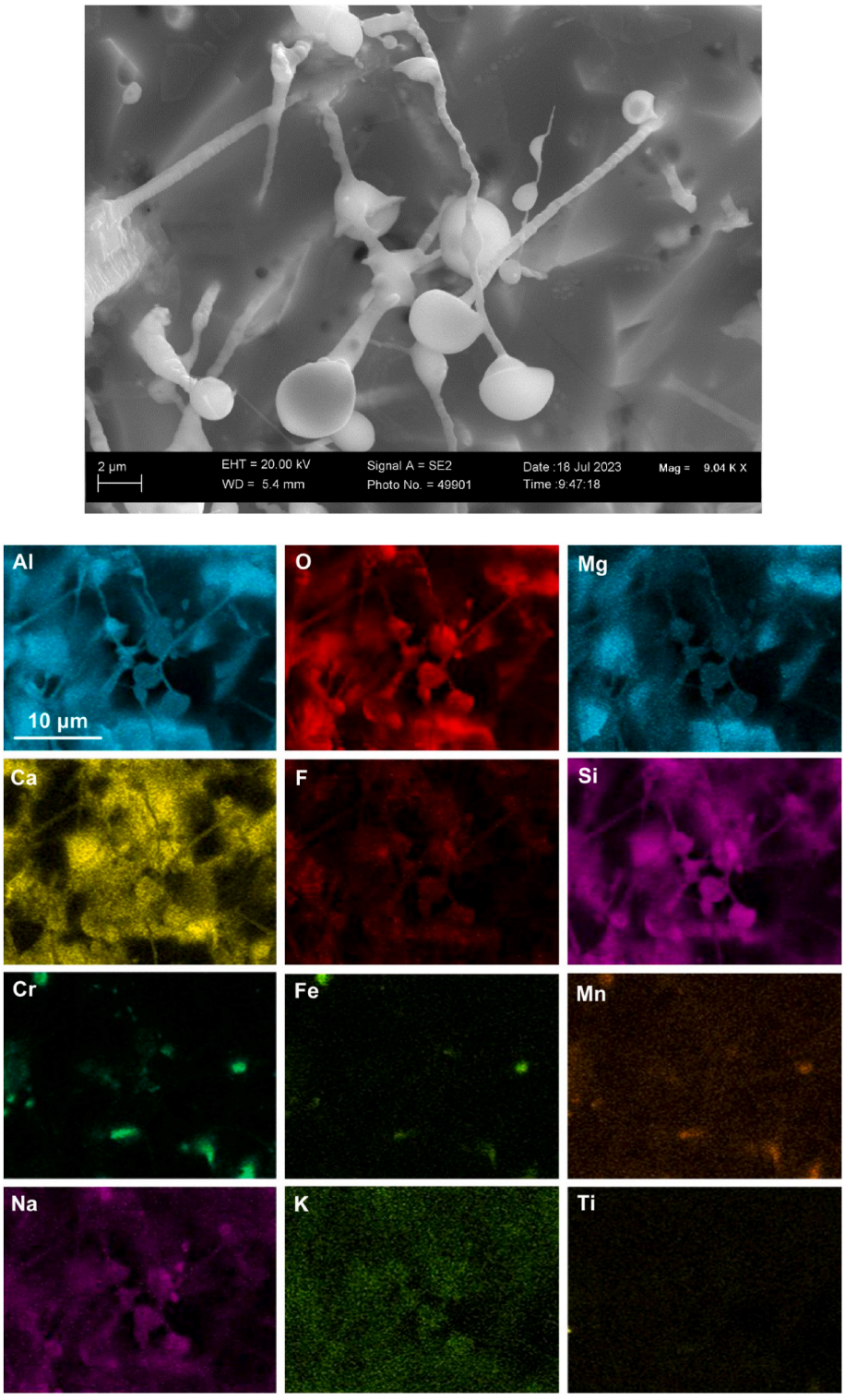

Fig. 8. (a): BSE image (x9040) of analysed area as marked in Fig. 7(a); (b): EDS map of area in Fig. 8(a).

gas phase containing metal vapour and fluorides. The information in Fig. 12 is useful since it shows that Al or Si metal will displace metal from the lesser stable fluorides in a reaction of the type displayed in reaction (4), [6–8,20]. Because of the different stoichiometries of metal to fluoride and phase changes across the temperature range, the generic reaction, as displayed in reaction (5), is derived from the sum of reactions (6) and (7). The Gibbs free energy calculation results for the displacement of metal by Al from the main metal fluorides (SiF_4, CrF_3, CrF_2, FeF_3, FeF_2) are shown in Fig. 15(a)-(c) for the formation of the different Al-fluorides: AlF, AlF_2 and AlF_3.

$$Al(g) + CrF_3(g) \leftrightarrow Cr(g) + AlF_3(g) \quad (4)$$

$$yAl + xMF_y \leftrightarrow xM + yAlF_x \quad (5)$$

$$yAl + xy/2F_2 \leftrightarrow yAlF_x \quad (6)$$

$$xMF_y \leftrightarrow xM + xy/2F_2 \quad (7)$$

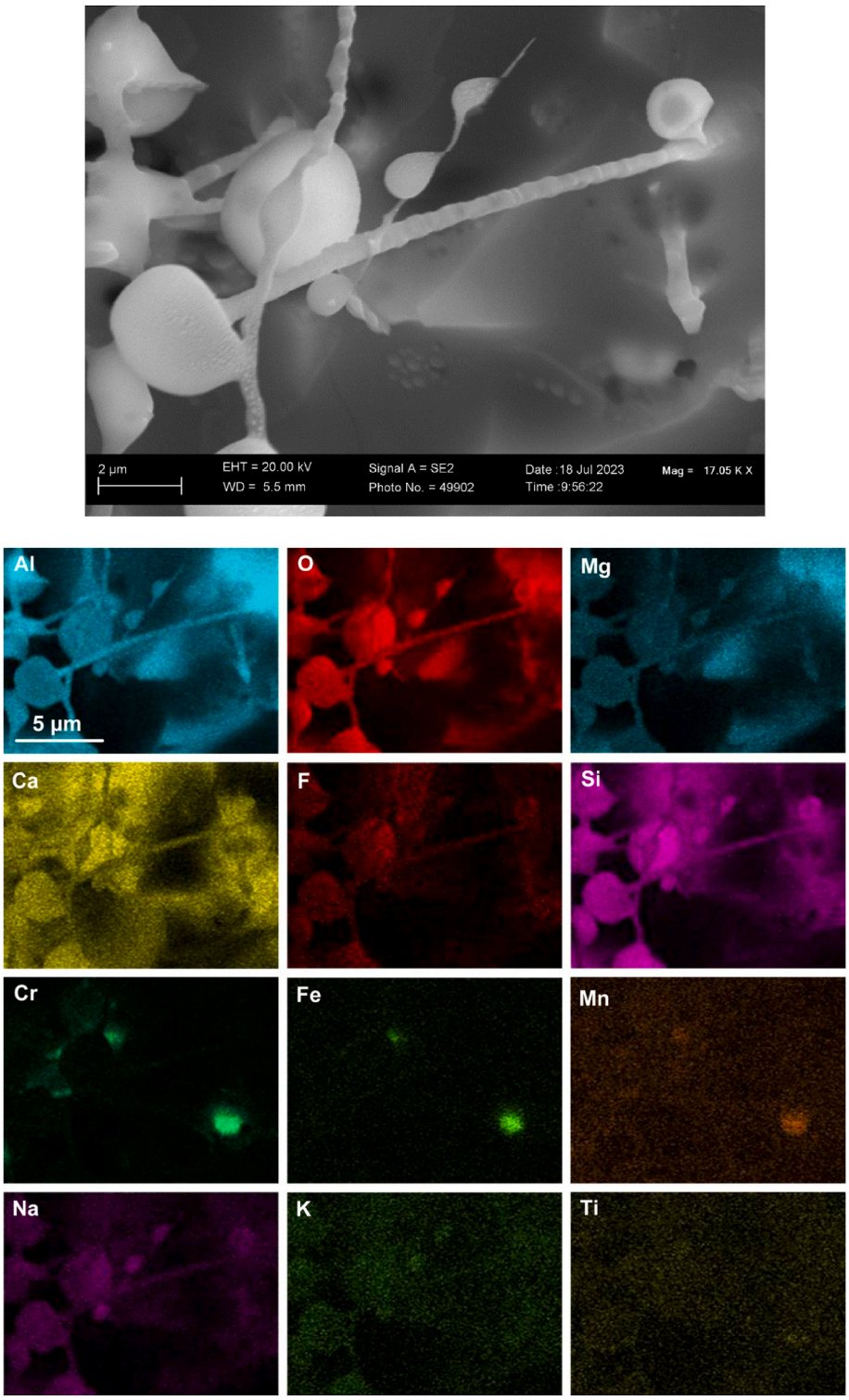

Fig. 9. (a):BSE image (x17050) of analysed area as marked in Fig. 7(a); (b): EDS map of area in Fig. 9(a).

Fig. 15(a)–(c) shows that all the main fluorides may react with Al to displace the metal as gas from the fluoride, with most of the lines sloping to lower Gibbs free energy values with increased temperature, indicating that these reactions are favoured by increased temperature. Only the lines for FeF_3 and CrF_3 in Fig. 15(c) show a slightly positive slope, indicating that increased temperature does not favour reaction (5) to displace Fe and Cr. The relative position of the lines in Fig. 15 indicates that Fe, Si, and Cr are most easily displaced as metal from their fluorides. Following metal displacement from their fluorides, the metal vapours will re-condensate upon cooling in the SAW process and transfer to the weld pool at the arc plasma-weld pool interface. This transfer pattern is also observed at the low reaction temperature applied here because chromium metal spots and patches of nano-scale were identified in the SEM work as confirmation of chromium transfer via the gas phase. The formation of CrF_2 is less probable than the formation of CrF_3, as shown in Figs. 12 and 14. The oxy-fluoride features in Figs. 2–10 confirm that Cr-fluorides did form from the pellet input materials. Therefore, the identification of the nano-strand phenomenon in this work, similar to

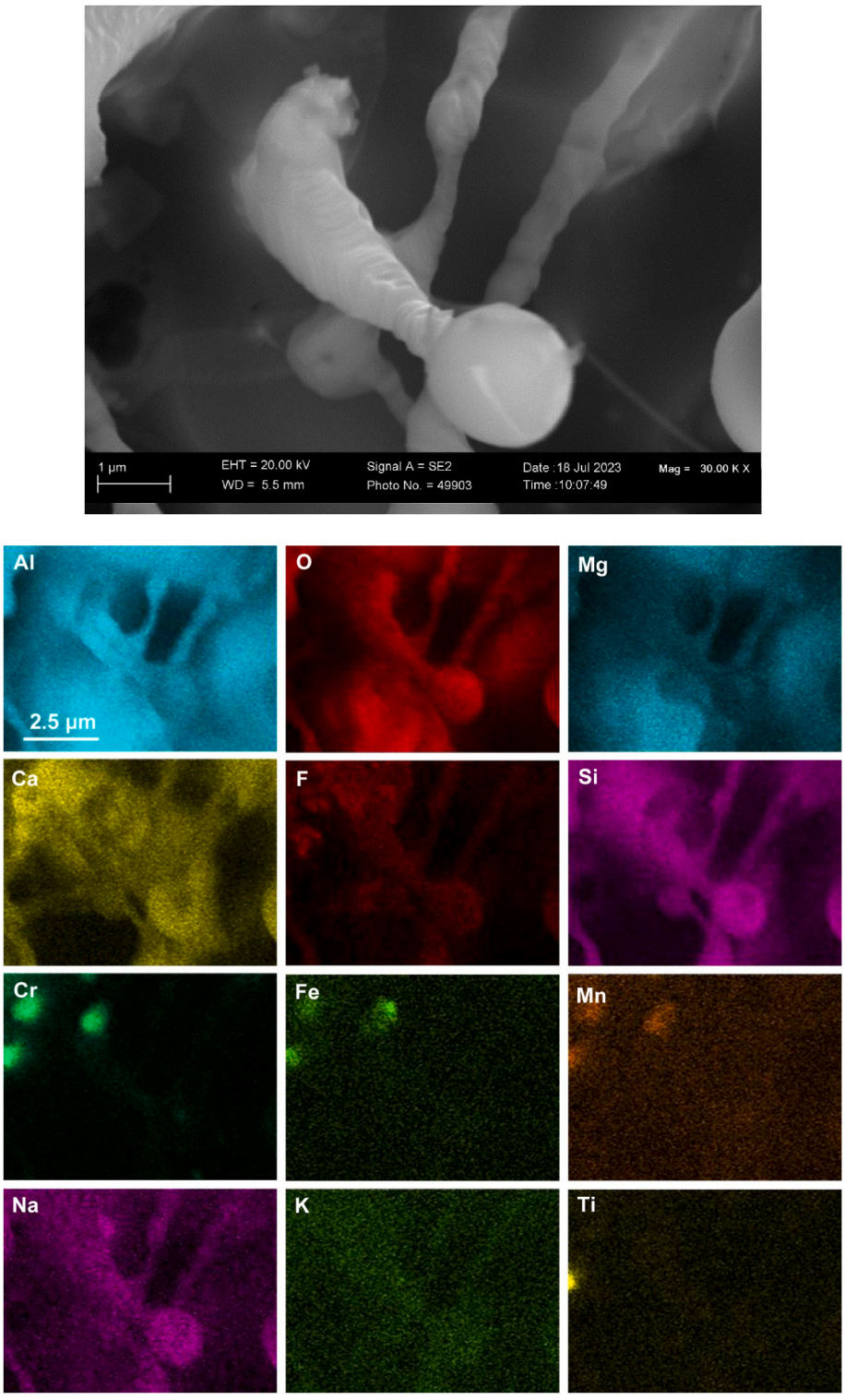

Fig. 10. (a): BSE image (x30000) of analysed area as marked in Fig. 7(a); (b): EDS map of area in Fig. 10(a).

those previously identified in post-weld slags, confirms fluoride vaporisation and re-condensation, even at the low temperature of 1350 °C which is much lower than 2000 °C–2500 °C in the arc cavity of the SAW process. The chromium element distribution patterns displayed in Fig. 2 (b) to 10(b) confirm that chromium is present in the oxy-fluoride features and also in metallic specs with Fe and Mn. In the authors' similar work on the reaction of Al–Ti–Fe metal powders with the same flux (see Table 1) and following the same experimental sequence at 1350 °C, the assimilation of Ti from the metal powder into oxy-fluoride nano-strands was confirmed [20]. The displacement of Ti from Ti-fluoride gas via reaction (5) and the re-condensation of metal vapour and fluoride gasses formed Ti-containing nano-strands. This reaction sequence can also explain the observations in this work on the assimilation of added Cr metal into oxy-fluoride nano-strands.

Table 2
Average EDS analysis of the field of view in Figs. 2–10.

Figure	%O	%F	%Na	%Mg	%Al	%Si	%K	%Ca	%Ti	%Cr	%Mn	%Fe
2	47.4	3.7	0.6	7.7	26.9	4.4	0.1	6.1	0.2	1.8	0.7	0.2
3	42.4	4.9	0.9	4.9	25.4	7.0	0.1	10.5	0.1	2.3	0.9	0.3
4	45.5	4.4	1.1	4.6	25.1	7.1	0.1	8.7	0.1	2.1	0.8	0.3
5	43.0	4.5	0.9	3.7	22.1	7.4	0.1	14.3	0.1	2.3	1.1	0.4
6	44.8	5.2	1.0	4.0	22.8	7.0	0.1	11.4	0.1	1.8	1.2	0.3
7	42.6	5.0	1.0	5.8	27.1	8.5	0.0	8.9	0.1	0.2	0.3	0.2
8	41.3	3.9	0.8	6.7	28.5	6.5	0.1	8.4	0.1	2.2	1.0	0.4
9	43.4	4.0	1.0	5.8	24.9	6.9	0.1	10.2	0.0	2.0	1.1	0.4
10	42.2	3.5	0.7	7.8	31.2	5.6	0.1	6.0	0.1	1.6	0.8	0.3
Maximum σ	0.43	0.12	0.02	0.07	0.25	0.07	0.01	0.09	0.07	0.03	0.02	0.02
Glass [12]	34.3	12.3	2.0	12.4	6.8	12.1	0.3	12.8	0.6	0.0	5.7	5.7
Glass [12]	34.1	12.7	2.0	12.3	6.2	12.4	0.0	13.3	0.7	0.0	5.8	5.8
Flux	35.3	8.7	0.6	13.4	13.2	9.2	0.2	9.3	0.6	0.0	5.3	4.2

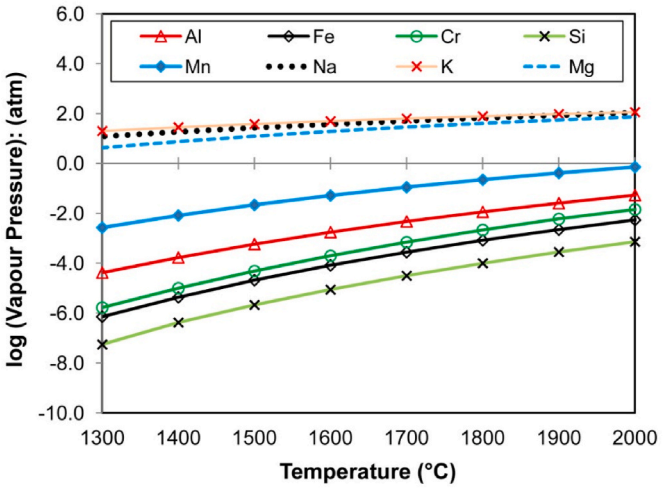

Fig. 11. Vapour pressure of metals (calculated in FactSage 7.3).

4. Conclusions

- SEM analyses identified oxy-fluoride nano-strands in the slag formed from the reaction of SAW flux and Al–Fe–Cr metal powders at 1350 °C.
- Chromium patches and spots of less than 1 μm scale formed part of the nano-strands, confirming that Cr assimilated via the gas phase.
- Thermochemical calculations were applied to discern the most probable reaction sequences for Cr assimilation and recovery from oxy-fluorides.
- Cr-fluoride formed part of the oxy-fluoride slag and likely formed Cr-fluoride gas. Cr was recovered via re-condensation of Cr gas formed from the reaction of Cr-fluoride with Al gas, added as Al metal powder.

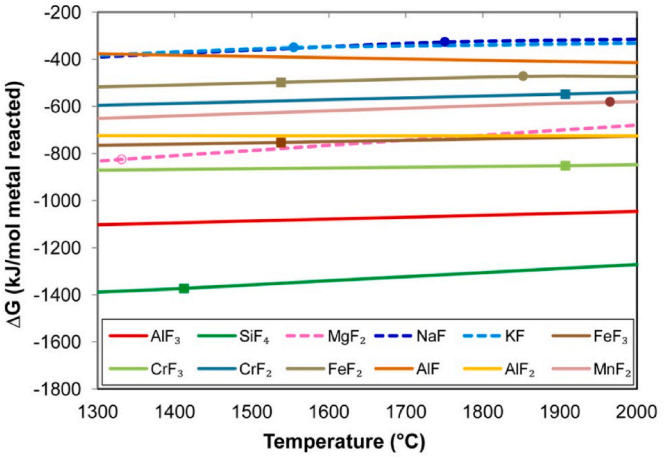

Fig. 12. Gibbs free energy of fluoride formation via reaction (1): open circle = $MF_X(s) \rightarrow MF_X(l)$; filled circle = $MF_X(l) \rightarrow MF_X(g)$; filled square = M(s)→M(l); dashed line = M(g).

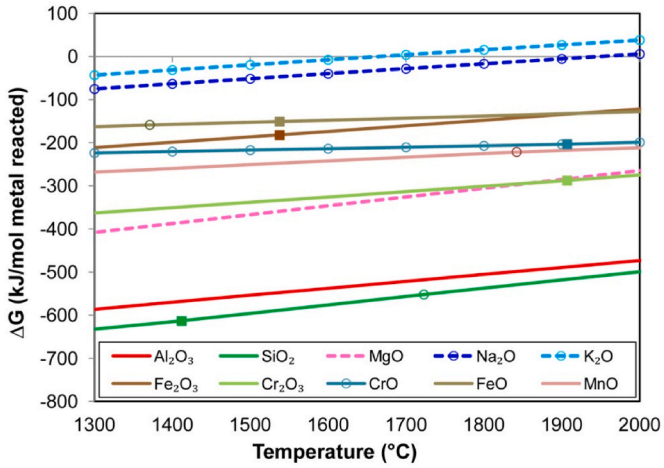

Fig. 13. Gibbs free energy of oxide formation via reaction (2): open circle = $M_xO_y(s) \rightarrow M_xO_y(l)$; filled square = M(s)→M(l); dashed line = M(g); open circles along the line = $M_xO_y(l)$ across the temperature interval.

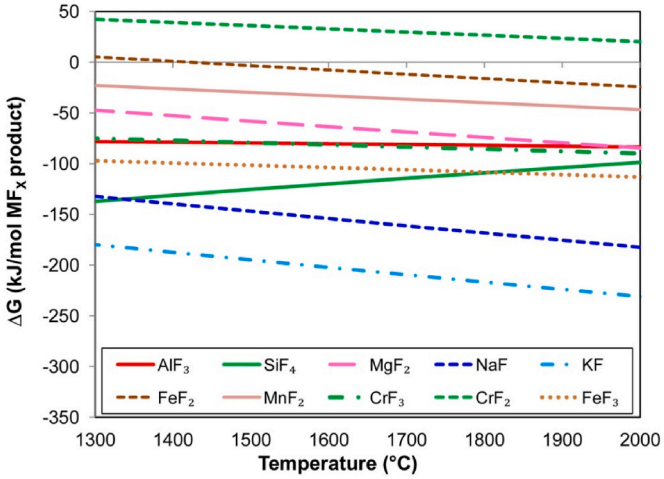

Fig. 14. Gibbs free energy of fluoride formation via reaction (3).

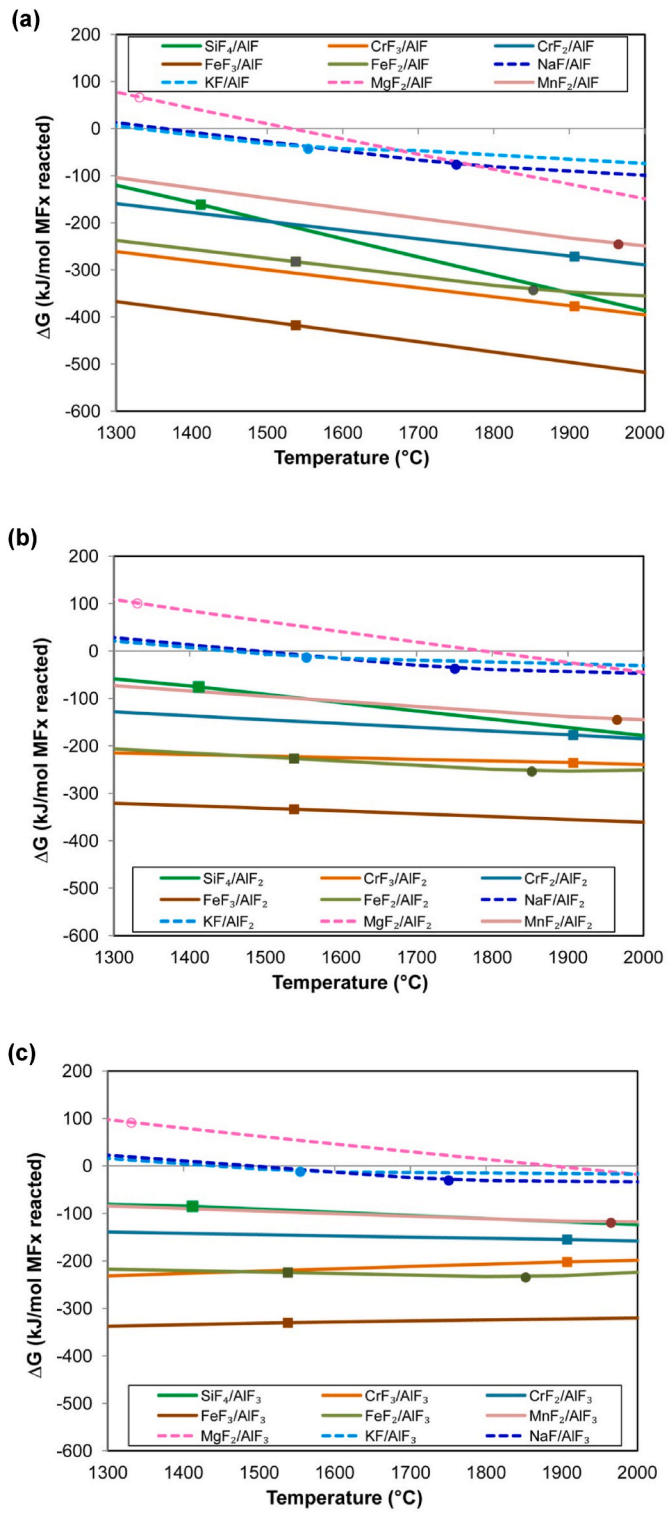

Fig. 15. (a): Gibbs free energy of element displacement via reaction (5) with AlF formation: open circle = $M_xO_y(s) \rightarrow M_xO_y(l)$; filled circle = $MF_X(l) \rightarrow MF_X(g)$; filled square = M(s)→M(l); dashed line = M(g)
Fig. 15(b): Gibbs free energy of element displacement via reaction (5) with AlF_2 formation: open circle = $M_xO_y(s) \rightarrow M_xO_y(l)$; filled circle = $MF_X(l) \rightarrow MF_X(g)$; filled square = M(s)→M(l); dashed line = M(g)
Fig. 15(c): Gibbs free energy of element displacement via reaction (5) with AlF_3 formation: open circle = $M_xO_y(s) \rightarrow M_xO_y(l)$; filled circle = $MF_X(l) \rightarrow MF_X(g)$; filled square = M(s)→M(l); dashed line = M(g).

- The simplified low temperature experimental method applied in this work can accurately simulate the gas phase-based reactions of the modified SAW process, namely gas formation and metal powder assimilation reactions.

Declaration of competing interest

The authors declare that they have no known competing financial interests or personal relationships that could have appeared to influence the work reported in this paper.

Acknowledgements

The University of Pretoria supported this work. The authors thank the following colleagues at the Laboratory for Microscopy and Microanalysis (University of Pretoria) for their advice and assistance on SEM imaging and analysis: Erna van Wilpe and Coenraad Snyman.

References

[1] Chai CS, Eagar TW. Slag-metal equilibrium during submerged arc welding. Metall Trans B 1981;12:539–47.
[2] Mitra U, Eagar TW. Slag-metal reactions during welding: Part 1. Evaluation and reassessment of existing theories. Metall Trans B 1991;22:65–71.
[3] Chai CS, Eagar TW. Slag metal reactions in binary CaF_2-metal oxide welding fluxes. Weld J 1982;61:229S–32S.
[4] Polar A, Indacochea JE, Blander M. Electrochemically generated oxygen contamination in submerged arc welding. Weld J 1990;69:68S–74S.
[5] Lau T, Weatherly GC, Mc Lean A. The sources of oxygen and nitrogen contamination in Submerged Arc Welding using CaO-Al_2O_3 based fluxes. Weld J 1985;69:343S–7S.
[6] Coetsee T, De Bruin F. Insight into the chemical behaviour of chromium in CaF_2-SiO_2-Al_2O_3-MgO flux applied in aluminium-assisted alloying of carbon steel in submerged arc welding. Minerals 2022;12:1397.
[7] Coetsee T, De Bruin F. Chemical behaviour of copper in the application of unconstrained Cr-Ni-Al-Cu metal powders in submerged arc welding: gas phase thermodynamics and 3D slag SEM evidence. Processes 2023;11:351.
[8] Coetsee T, De Bruin F. EERZ (effective equilibrium reaction zone) model of gas-slag-metal reactions in the application of unconstrained Al-Ni-Cr-Co-Cu metal powders in submerged arc welding: model and 3D slag SEM evidence. Processes 2023;11:2110.
[9] Coetsee T, De Bruin F. Reactions at the molten flux-weld pool interface in submerged arc welding. High Temp. Mater Process 2021;40:421–7.
[10] Coetsee T, De Bruin FJ. Improved titanium transfer in Submerged Arc Welding of carbon steel through aluminium addition. Miner Process Extr Metall Rev 2021;43:771–4.
[11] Coetsee T, Mostert RJ, Pistorius PGH, Pistorius PC. The effect of flux chemistry on element transfer in Submerged Arc Welding: application of thermochemical modelling. Mater. Res. Technol. 2021;11:2021–36.
[12] Coetsee T. Phase chemistry of Submerged Arc Welding (SAW) fluoride based slags. Mater. Res. Technol. 2020;9:9766–76.
[13] Bale CW, Bélisle E, Chartrand P, Decterov S, Eriksson G, Gheribi AE, Hack K, Jung I-H, Kang Y-B, Melançon J, et al. Reprint of: FactSage thermochemical software and databases, 2010–2016. Calphad 2016;55:1–19.
[14] Coetsee T, De Bruin F. Aluminium-assisted alloying of carbon steel in submerged arc welding with Al-Cr-Ni unconstrained metal powders. Processes 2022;10:2265.
[15] Hallén H, Johansson K-E. Use of a metal powder for surface coating by submerged arc welding. U.S. Patent 6331688 2001;B1.
[16] Lau T, Weatherly GC, Mc Lean A. Gas/Metal/Slag reactions in Submerged Arc Welding using CaO-Al_2O_3 based fluxes. Weld J 1986;70:31S–8S.
[17] Schultz T, Lychatz B, Haustein N, Janke D. Structurally based assessment of the influence of fluorides on the characteristics of continuous casting powder slags. Metall Trans B 2013;44:317–26.
[18] Gao J, Wen G, Liu Q, Tan W, Tang P. Effect of Al_2O_3 on the fluoride volatilization during melting and ion release in water of mould flux. J Non-Cryst Solids 2015;409:8–13.
[19] Zaitsev AI, Leites AV, Litvina AD, Mogutnov BM. Investigation of the mould powder volatiles during continuous casting. Steel Res 1994;65:368–74.
[20] Coetsee T, De Bruin FJ. Nano-strand formation in CaF_2-SiO_2-Al_2O_3-MgO flux reacted at 1350 °C with Al-Ti-Fe powder: SEM analyses and gas reaction thermochemistry. J Solid State Chem 2024;331:124547.